Astrophys Space Sci (2014) 351:67–73
DOI 10.1007/s10509-014-1820-3

ORIGINAL ARTICLE

Determination of coronal magnetic fields from 10 to $26R_{\odot}$ using the density compression ratios of CME-driven shocks

A. Shanmugaraju · K. Suresh · Y.-J. Moon

Received: 28 October 2013 / Accepted: 27 January 2014 / Published online: 12 February 2014

Abstract Recently, the estimation of coronal magnetic field using new methods, such as standoff distance method or density compression ratio method has been reported. In the present work, we utilized the density compression ratio of CME-driven shocks for 10 events at 29 different locations in the upper solar corona (10–$26R_{\odot}$) and determined the coronal magnetic field for two different adiabatic indices ($\gamma = 4/3$ and $5/3$). In addition, radial dependence of shock parameters in the corona is studied. It is found that the magnetic field estimated in the above range agree with the general trend. In addition, we obtained a radial profile of magnetic field [$B(R) = 623R^{-1.4}$] in the entire upper corona (3–$30R_{\odot}$) by combining the magnetic field estimated by Kim et al. (Astrophys. J. 746:118, 2012) in the range 3–$15R_{\odot}$ and that estimated in the present study in the range (10–$26R_{\odot}$). The power-law indices are nearly in agreement with recent results of CME-driven shocks reported in the literature. The results are discussed with the comparison of newly reported coronal magnetic field values obtained by different techniques and found that the power-law relation closely follow the literature values.

Keywords Sun · Coronal mass ejection · Shock waves · Magnetic field

A. Shanmugaraju
Arul Anandar College, Madurai 625514, Tamilnadu, India
e-mail: ashanmugaraju@gmail.com

K. Suresh (✉)
Madurai Kamaraj University, Madurai 625021, Tamilnadu, India
e-mail: suresh66066@yahoo.com

Y.-J. Moon
School of Space Research, Kyung Hee University,
Yongin 446-701, Korea
e-mail: moonyj@khu.ac.kr

1 Introduction

The solar corona is the outer most atmosphere of the sun being above the chromospheres. It consists of plasma and million Kelvin. Recent observations of coronal mass ejections (CMEs) and their associated shock signatures by the LASCO on board the SOHO satellite (Brueckner et al. 1995) enable us to study the physical properties of solar corona and the erupting features. For example, the coronal magnetic field (not measurable directly) is important to be studied for understanding the formation of shocks. On the other hand, several authors (e.g., Smerd et al. 1974) adopted the band splitting observed in metric type II radio burst to determine the coronal magnetic field (Cho et al. 2007). Vrsnak et al. (2004) used this technique to determine Interplanetary (IP) magnetic field from band splitting in IP type IIs. Several other techniques have been used to determine the coronal magnetic field at the base of the corona in Microwave and Infrared wavelengths (Lin et al. 2000; Lee, 2007), extrapolation technique (e.g., Wiegelmann 2008), and Faraday rotation technique (Patzold et al. 1987; Spangler 2005; Ingleby et al. 2007) and method using radio data (Lee et al. 1999; Ramesh et al. 2010). In addition, white-light shock structure of CMEs have been observed in coronagraph imager (Sheeley et al. 2000; Vourlidas et al. 2003). From the CME-driven shock signatures seen in combined white-light and EUV data, Bemporad and Mancuso (2010) derived many plasma parameters including the magnetic field.

In a new methodology, the shock standoff distance in front of the CME front has been used to calculate the coronal magnetic field by Gopalswamy and Yashiro (2011). The shock signature was seen well ahead of CME front on 25 March 2008 and they deduced a magnetic field of ≈48 mG at $6R_{\odot}$ ($R_{\odot}$ = one solar radius) and it reduces to

8 mG at $23R_{\odot}$. Hence they obtained a power law form as $B(r) = pr^{-q}$. They compared this trend with that of Dulk and Mclean (1978) and Patzold et al. (1987). This work was followed by Kim et al. (2012) for 10 fast CMEs, and they estimated the magnetic field (105–6 mG) at a heliocentric distance range 3–$15R_{\odot}$. They also used density compression ratio (ρ_2/ρ_1 = up-stream/down-stream electron density) for estimating the coronal magnetic field. On the other hand, Eselevich and Eselevich (2011) analyzed shock parameters using SOHO/LASCO C3 observation. Mainly they examined shock discontinues in front of the CMEs and found the dependence of Alfven Mach number on the density compression ratio (ρ_2/ρ_1), shock strength at distances greater than $10R_{\odot}$ from the center of the sun. Motivated by the results of Gopalswamy and Yashiro (2011) and Kim et al. (2012), we utilized the value of compression ratio of the 10 events measured by Eselevich and Eselevich (2011) in the distance range 10–$26R_{\odot}$ and the corresponding coronal magnetic field is determined in the present study as described in Kim et al. (2012).

Gopalswamy and Yashiro (2011) obtained the coronal magnetic field profile over a distance range 6–$23R_{\odot}$ for a single event, whereas, Gopalswamy et al. (2012) measured the magnetic field in the inner corona ($\sim 1.4R_{\odot}$) for another event using standoff distance method. Kim et al. (2012) applied this method and density compression ratio method for 10 CMEs, and they obtained magnetic field in the range 3–$15R_{\odot}$. On the other hand in the present study, the coronal magnetic field in the upper corona 10–$26R_{\odot}$ is determined using density compression ratio of 10 CMEs at 29 different locations in the above range. The data set is also different from Kim et al. (2012) except one event on July 1999. While Kim et al. (2012) data covers the period up to October 2003, five events in the present study cover the period from November 2003 to March 2008.

While Eselevich and Eselevich (2011) obtained the density compression ratios of the 10 events, we have extended that work to estimate the magnetic field in the upper corona. In addition, we compare the results with the reported magnetic field values found out using the new method of standoff distance and density compression ratio (Bemporad and Mancuso 2010; Gopalswamy and Yashiro 2011; Kim et al. 2012; Gopalswamy et al. 2012; Poomevises et al. 2012), and with recently reported values estimated by other means (Ramesh et al. 2010; Ma et al. 2011; Vasanth et al. 2013). The data and method adopted are described in Sect. 2. The results, radial dependence of magnetic field and shock parameters obtained in the present study along with the comparison of recent results are presented in Sect. 3. A brief conclusion is presented in Sect. 4.

2 Data and method

Eselevich and Eselevich (2011) analyzed shock parameters using SOHO/LASCO C3 observation. Mainly they examined shock discontinues in front of the CMEs and found the dependence of Alfven Mach number on the density compression ratio (ρ_2/ρ_1), shock strength at distances greater than $10R_{\odot}$ from the center of the sun. They calculated the density jump (δN) from the brightness jump (δP) observed in the LASCO C3 imager. The density compression ratio was obtained by them using the relation $\frac{\rho_2}{\rho_1} = 1 + \frac{\delta N}{N_O}$. Where N_0 is the electron density of the unperturbed plasma preceding the shock front. We utilized the value of compression ratio of the 10 events measured in the distance range 10–$26R_{\odot}$. As described by Kim et al. (2012), the Mach number can be calculated from the relation,

$$M^2 = \frac{2\rho_2/\rho_1 + \gamma + 1}{\gamma + 1 - \rho_2/\rho_1(\gamma - 1)} \tag{1}$$

Using this Mach number representing the shock strength, the Alfven speed (V_A) and B are estimated as,

$$V_A = V_{SH}/M \tag{2}$$

$$B = 0.5 \times 10^{-6} V_A \rho^{0.5} \tag{3}$$

where V_{SH} is the shock speed reported by Eselevich and Eselevich (2011), γ is the adiabatic index and ρ is the upstream density.

In order to obtain the upstream plasma density (ρ), we used the Saito et al. (1977) and Leblanc et al. (1998) models. The coronal magnetic field values estimated for the 10 events at 29 different locations in the heliocentric distance between 10–$26R_{\odot}$ are represented in Fig. 1 (top—for *Leblanc* model) along with the known coronal magnetic field profiles of Dulk and Mclean (1978) and Mann et al. (1999). The variation of magnetic field in the distance range 10–$26R_{\odot}$ is clearly seen in Fig. 1 i.e., the coronal magnetic field decreases as the distance increases, which is in agreement with that of the earlier reports.

Similarly, the magnetic field values obtained using *Saito model* are plotted in Fig. 1 (bottom panel). The results are shown for two different adiabatic indices 4/3 (marked as diamonds) and 5/3 (marked as circles). Except for two locations, the estimated values follow closely the profiles of Dulk and Mclean (1978) and Mann et al. (1999). Also, a power-law fit (drawn as thin line) to the estimated magnetic field (in Gauss) values is obtained as,

$$B(R) = 0.887R^{-1.53} \tag{4}$$

which is slightly different from that obtained for a single event by Gopalswamy and Yashiro (2011) in the range 6–$23R_{\odot}$. As seen in Fig. 1 (bottom panel), the magnetic field

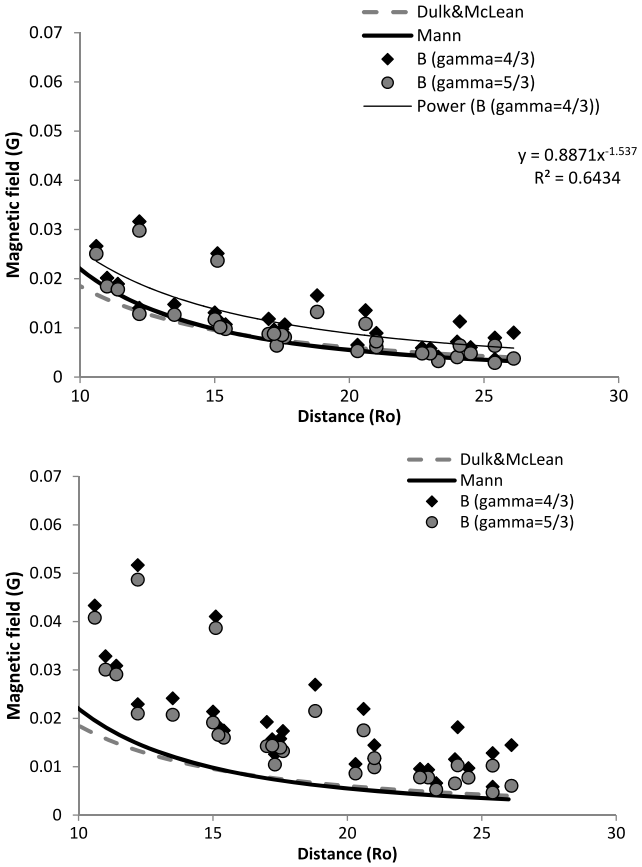

Fig. 1 The coronal magnetic field for the 10 events in the heliocentric distance between 10–26$R_\odot$ estimated from density compression ratio utilizing Leblanc model (*top*) and Saito model (*bottom*). The coronal magnetic field profiles of Mann et al. (1999) and, Dulk and Mclean (1978) are also shown for comparison. A power-law fit (*thin line*) is drawn in the top panel

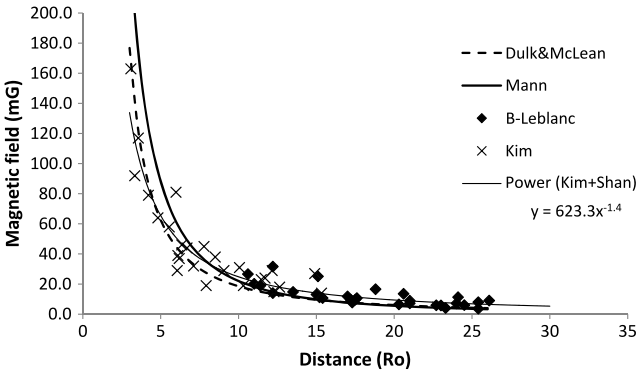

Fig. 2 Plot shows the magnetic field obtained in the present study (in the distance range 10–26$R_\odot$) along with that of Kim et al. (2012) in the distance range 3–15$R_\odot$. The combined data is fitted with a power-law (*thin line*) to obtain a radial profile of the magnetic field in the entire upper corona 3–30$R_\odot$

values obtained when Saito model is utilized for upstream plasma density deviate more from the profiles of Dulk and Mclean (1978) and Mann et al. (1999).

The uncertainty in the determination of magnetic field can be noted as follows. As described above, based on the density models used for upstream plasma density, the value of magnetic field varies. For example, the magnetic field values derived using Saito model are higher than that using Leblanc model. Also, it is evident from the Fig. 1 that the deviation between the two values is larger in the lower corona ($\sim 10R_\odot$) than the deviation in the upper corona ($\sim 25R_\odot$). But, as seen from the two plots of Fig. 1, the magnetic field values obtained utilizing the Leblanc model are in agreement to the literature values (Dulk and Mclean 1978; Mann et al. 1999).

Further, as given by Eselevich and Eselevich (2011), the uncertainty in locating the shock discontinuity is $\sim 0.1R_\odot$ if the shock front is located within $\pm 10^o$ from the direction of CME leading edge. For all the 10 events, they noted the shock discontinuity in the differential brightness image near the direction of CME propagation within $\pm 10^o$. The error of $0.1R_\odot$ in height leads to different density in the corona. For example, the density at $10R_\odot$ using Leblanc model is 3790 cm^{-3}, whereas, it is 3704 cm^{-3} at $10.1R_\odot$. In the magnetic field expression ($B = 0.5 \times 10^{-6} V_A \rho^{0.5}$), because of the square root of density term, the error will be very minimum. If the uncertainty in locating the shock discontinuity is $\sim 0.2R_\odot$, then the density at $10.2R_\odot$ is 3621 cm^{-3} and the magnetic field estimated at $10R_\odot$ should be multiplied by a factor of $\sim 1.4 (= \sqrt{3790} - \sqrt{3621})$.

On the other hand, the error in estimation of magnetic field arises due to the assumption of particular density model for upstream plasma density and also due to the usage of adiabatic index value. For example, as seen from Fig. 1, using the Leblanc model gives a maximum value of 0.032 G, whereas, it is 0.052 G in using Saito model for an adiabatic index of 4/3. That is, Saito model gives nearly 60 % higher value than the Leblanc model. In using the different adiabatic indices (4/3 and 5/3), the deviation is found (less than 10 %) around 0.002 G in Leblanc and Saito models.

3 Results

3.1 Radial magnetic field profile

Next, we combined the results (for $\gamma = 4/3$) of present study with the magnetic field values obtained by Kim et al. (2012) using density compression ratio to obtain a radial profile of the magnetic field in the entire upper corona 3–30$R_\odot$. As mentioned earlier, Kim et al. (2012) covered a distance range of 3–15$R_\odot$ and the present study covers a distance range of 10–26$R_\odot$, and there is a nice over lap of 5$R_\odot$. Hence, it is possible for us to get a radial profile of coronal magnetic field (in mG) as a power law relation ($623R^{-1.4}$) as shown in Fig. 2. It is interesting to note that the power law

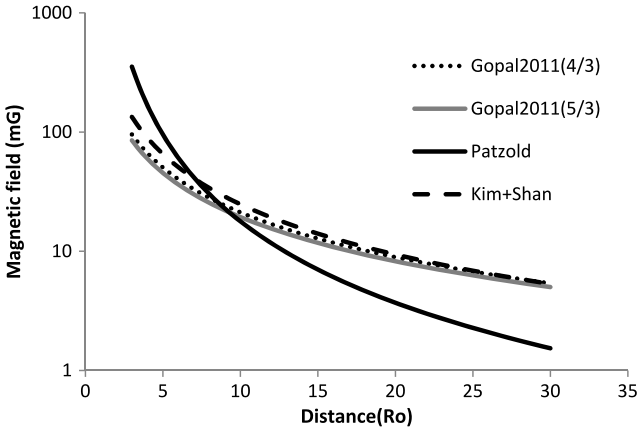

Fig. 3 Plot shows the radial dependence of coronal magnetic field obtained in the present study along with that of Gopalswamy and Yashiro (2011) (for two different values of adiabatic indices $\gamma = 4/3$ and $5/3$) and Patzold et al. (1987) in the height range of 3–30$R_{\odot}$

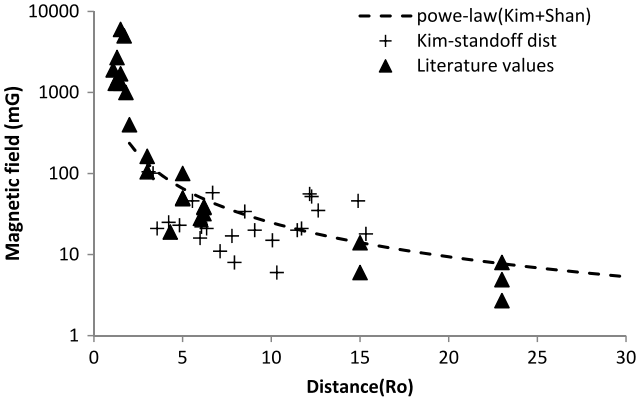

Fig. 4 Plot shows the comparison of the coronal magnetic field curve obtained in the present study with the reported values (marked as *triangles*) at different distances in Table 1. The *plus symbols* denote the values obtained by Kim et al. (2012) using the standoff distance method

fit closely follow the both the profiles of Dulk and Mclean, and Mann et al. The slight difference in the lower region reduces in the upper region nearly after $12R_{\odot}$.

As shown in Fig. 3, the power law model derived in the present study is compared with that of Gopalswamy and Yashiro (for two different values of adiabatic indices $\gamma = 4/3$ and $5/3$) along with the curve of Patzold et al. (1987). The radial magnetic field curve (pR^{-q}) obtained in the present study lies very close to that of Gopalswamy and Yashiro (2011), but deviates from Patzold et al. (1987) at greater heights (as similar to the results of Gopalswamy and Yashiro 2011). Note that, now the power law indices obtained by us ($p = 623$ and $q = -1.4$) for the entire upper corona are in close agreement with that of Gopalswamy and Yashiro (2011).

In Fig. 4, the recently reported values of coronal magnetic field in the upper corona ($<30R_{\odot}$) obtained using different techniques are shown along with the power law curve. It can be seen that the trend of radial dependence of coronal magnetic field obtained in the present study nicely follows the literature values. But, the power-law curve is less steeper so that some of the points lie below the curve. As suggested by Kim et al. (2012), this slight deviation might be due to the excess values of magnetic field estimated by the density compression ratio method. The coronal magnetic field values determined and reported by many authors are listed in Table 1. The name of author, distance, magnetic field and technique are presented in column 1–4, respectively.

In order to obtain a relation for heliospheric magnetic field, we considered the results of Vrsnak et al. (2004) and Poomevises et al. (2012) along with that of Helios data (as given in Poomevises et al. 2012). Vrsnak et al. (2002, 2004) obtained the coronal and interplanetary magnetic field using the band splitting seen in metric and interplanetary type II bursts and compared their results with published values. They found that the magnetic field in the inner corona ($1.3 < R < 3$) follows like R^{-3} to R^{-4} and follows as R^{-2} beyond this range yielding 5 nT at 1 AU. On the other hand, recently, Poomevises et al. (2012) used the standoff distance method of CME-driven shock in the coronal and interplanetary regions and obtained 28 mG at $6R_{\odot}$, and 0.17 mG at 120 $R_{\odot}$. We utilized the magnetic field values reported in the inner heliosphere to obtain the relation for heliospheric magnetic field as $2561R^{-2.1}$ as shown in Fig. 5. Note that this relation is similar to $2433R^{-2.09}$ of Poomevises et al. obtained using Saito model and $2111.5R^{-2.05}$ using Leblanc model for $\gamma = 5/3$. The relations obtained by them ($706R^{-1.54}$ for $\gamma = 4/3$ using Leblanc model, $524.727R^{-1.75}$ for Helios observations) and $623R^{-1.4}$ obtained in the present study for upper corona are shown in Fig. 5 for comparison.

The above observational results can be explained using theoretical argument on the radial profile of magnetic fields. We can consider two cases as follows. The first case is a diverging flux tube in which $BA = constant$, where A is the cross sectional area of the flux tube. If the size of the flux tube linearly increase with the distance from the sun, one can obtain the magnetic field as, $B \propto R^{-2}$. The second case is the expansion of a magnetic cloud in which $\int \frac{B^2}{8\pi} dv = constant$, where $\frac{B^2}{8\pi}$ is magnetic energy density. If the cloud has a self-similar expansion, the magnetic field is proportional to $R^{-1.5}$.

3.2 Radial dependence of shock parameters

In addition, the variation of shock parameters like density compression ratio, shock speed, Mach number and Alfven speed over coronal distances are examined as shown in the following Figs. 6 and 7. Among these, the former two parameters were obtained by Eselevich and Eselevich (2011) and the latter two parameters are obtained in the present

Table 1 List of literature results of coronal and heliospheric magnetic field

Name of the author	Distance ($R_\odot$)	Magnetic field (mG)	Method
Bemporad and Mancuso (2010)	4.3	19	Density compression ratio
Cho et al. (2007)	1.5	1300	Band splitting
	2	400	
Dulk and Mclean (1978)	23	4.9	Model
Gopalswamy and Yashiro (2011)	5	50	Standoff distance
	6.2	38	
	23	8	
Gopalswamy et al. (2012)	1.2	1500	Standoff distance & Band splitting
	1.35	1300	
Ingleby et al. (2007)	5	49	Faraday rotation
	6.2	32	
Kim et al. (2012)	3	110	Standoff distance
	15	6	
	3	160	Density compression ratio
	15	14	
Ma et al. (2011)	1.25	1300	Band splitting
Mann et al. (1999)	1.08	1900	EIT wave
	1.8	1000	
Patzold et al. (1987)	23	2.7	Faraday rotation
	5	100	
Poomevises et al. (2012)	6	28	Standoff distance
	120	0.17	
Ramesh et al. (2010)	1.5	6000	Radio observation
	1.7	5000	
Spangler (2005)	6.2	39	Faraday rotation
Vasanth et al. (2013)	1.3	2700	Band splitting
	1.5	1700	
Vrsnak et al. (2002)	1.6	1000–8000	Band splitting
	2.5	300–900	
Vrsnak et al. (2004)	215	0.05	Band splitting

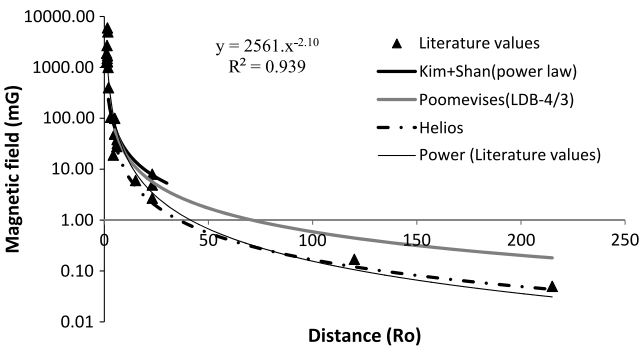

Fig. 5 Similar to Fig. 4, but in the entire the heliospheric distance range. The magnetic field values at $120R_\odot$ and at 1 AU (as listed in Table 1) are included in this figure (see text for more details)

study. As seen in Fig. 6a, the density compression ratio increases with distance. As already noted by Kim et al. (2012) where they found a slightly decreasing trend, the increasing trend is in contrast with them. On the other hand, our results are in agreement with that of Ontivores and Vourlidas (2009). In order to check this opposite trends, we included the results of Ontivores and Vourlidas (2009) in Fig. 6a for comparison, and there exists a slight positive correlation in their data similar to our results. Note that Ontivores and Vourlidas (2009) obtained density compression ratio for halo CMEs. This means that real values of R should be larger (about 1.3–1.5 times) and the light triangles in Fig. 6 (upper panel) should be slightly shifted to the right. Qualitatively, the dependence remains almost the same. Similarly, the Mach number determined in the present study also increases with respect to distance as seen in Fig. 6b.

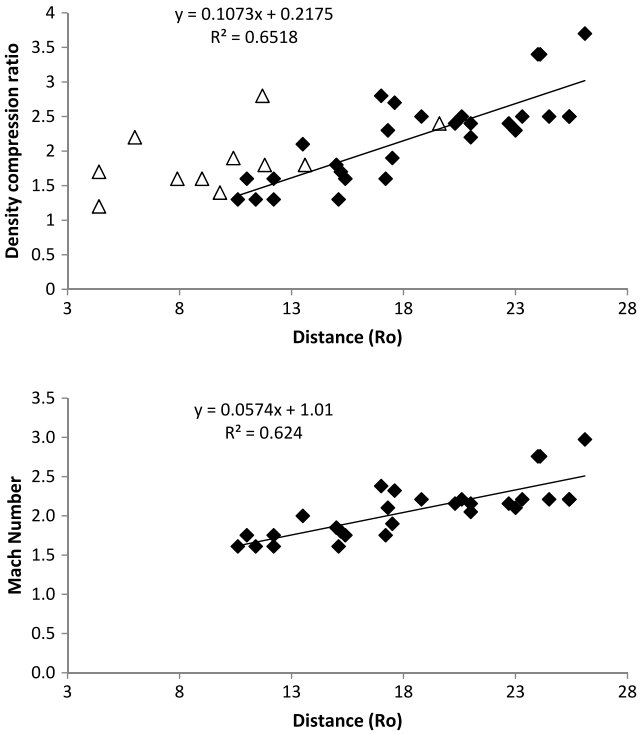

Fig. 6 Radial dependence of density compression ratio (*top panel*). The density compression ratio values obtained by Ontivores and Vourlidas (2009) are also shown for comparison in the *top panel*. Straight line is the linear fit (*bottom panel*). Radial dependence of Mach number determined using $\gamma = 4/3$

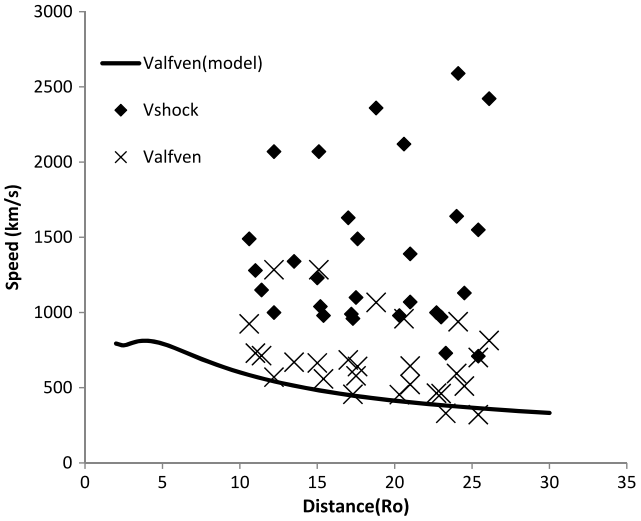

Fig. 7 Radial dependence of shock speed reported by Eselevich and Eselevich (2011) and Alfven speed estimated in the present study using Eq. (2). The Alfven speed curve obtained using model values is also shown (*thick line*)

The radial dependence of shock speed and Alfven speed are shown in Fig. 7 along with the Alfven speed curve determined utilizing the Leblanc density model, and, Dulk and McLean magnetic field model in the relation $V_A = 0.5 \times 10^{-6} B\rho^{-0.5}$. As seen in this plot, the shock speed determined by Eselevich and Eselevich (2011) are well above the Alfven speed curve and many of the Alfven speed values estimated in the present study (using Eq. (2)) for the 10 events are just above curve. It implies that the shocks are strong and super-Alfvenic for all these events. This result is similar to that of Kim et al. (2012).

4 Conclusion

We have extended the work of Eselevich and Eselevich (2011) to estimate the magnetic field in the upper corona (10–26$R_\odot$) utilizing the density compression ratios of CME-driven shocks of 10 events at 29 different locations. We found that the magnetic field values and the trend are in agreement with that of Dulk and Mclean (1978) and Mann et al. (1999). A power-law relation is obtained by combining the values of Kim et al. (2012) and the values obtained in the present study covering the entire upper corona (3–30$R_\odot$). The magnetic field profile drawn using this power-law relation closely follows the profile of Gopalswamy and Yashiro (2011).

In addition, we compared the results with literature values and they are found to be within the range of reported magnetic field values obtained using the new method of standoff distance and density compression ratio (Bemporad and Mancuso 2010; Gopalswamy and Yashiro 2011; Kim et al. 2012; Gopalswamy et al. 2012; Poomevises et al. 2012), and with recently reported values estimated by other means (Ramesh et al. 2010; Ma et al. 2011; Vasanth et al. 2013).

From the Mach numbers estimated, they are within the acceptable range 1.3–3.7. The shocks are found to be strong and super-Alfvenic. Radial dependence of shock parameters (density compression ratio, shock speed, Mach number and Alfven speed) is studied and found that the density compression ratio increases with the distance in contrast to Kim et al. (2012), but in agreement to Ontivores and Vourlidas (2009).

Acknowledgements We are grateful to the Solar Geophysical Data team for their open data policy. The CME catalog we have used is generated and maintained by the Center for Solar Physics and Space Weather, The Catholic University of America in cooperation with the Naval Research Laboratory and NASA. SOHO is a project of international cooperation between ESA and NASA. The grant to A.S. from University Grants Commission, Govt. of India, through major research project F. No. 42-845/2013 (SR) is kindly acknowledged.

References

Bemporad, A., Mancuso, S.: Astrophys. J. **720**, 130 (2010)
Brueckner, G.E., Howard, R.A., Koomen, M.J., Korendyke, C.M., Michels, D.J., Moses, J.D., Socker, D.G., Dere, K.P., Lamy, P.L.,

Llebaria, A., Bout, M.V., Schwenn, R., Simnett, G.M., Bedford, D.K., Eyles, C.J.: Sol. Phys. **162**, 357 (1995)
Cho, K.S., Lee, J., Gary, D.E., Moon, Y.J., Park, Y.D.: Astrophys. J. **665**, 799 (2007)
Dulk, G.A., Mclean, D.J.: Sol. Phys. **57**, 279 (1978)
Eselevich, M., Eselevich, V.: Astron. Rep. **55**, 359 (2011)
Gopalswamy, N., Yashiro, S.: Astrophys. J. **736**, L17 (2011)
Gopalswamy, N., Nitta, N., Akiyama, S., Makela, P., Yashiro, S.: Astrophys. J. **744**, 72 (2012)
Ingleby, L.D., Spangler, S.R., Whiting, C.A.: Astrophys. J. **668**, 520 (2007)
Kim, R.S., Gopalswamy, N., Moon, Y.J., Cho, K.S., Yashiro, S.: Astrophys. J. **746**, 118 (2012)
Leblanc, Y., Dulk, G.A., Bougeret, J.L.: Sol. Phys. **183**, 165 (1998)
Lee, J.: Space Sci. Rev. **133**, 73 (2007)
Lee, J., White, S.M., Kundu, M.R., Mikic, Z., McClymont, A.N.: Astrophys. J. **510**, 413 (1999)
Lin, H., Penn, M.J., Tomczyk, S.: Astrophys. J. **541**, L83 (2000)
Ma, S., Raymond, J.C., Golub, L., Lin, J., Chen, H., Grigis, P., Testa, P., Long, D.: Astrophys. J. **738**, 160 (2011)
Mann, G., Aurass, H., Klassen, A., Estel, C., Thompson, B.J.: In: Vial, J.-C., Kaldeich-Schümann, B. (eds.) 8th SOHO Workshop, Plasma Dynamics and Diagnostics in the Solar Transition Region and Corona (ESA SP-446), p. 477. ESA, Noordwijk (1999)
Ontivores, A., Vourlidas, A.: Astrophys. J. **693**, 267 (2009)
Patzold, M., Bird, M.K., Volland, H.: Sol. Phys. **109**, 91 (1987)
Poomevises, W., Gopalswamy, N., Yashiro, S., Kwon, R.-Y., Olmedo, O.: Astrophys. J. **758**, 118 (2012)
Ramesh, R., Kathiravan, C., Sastry, C.V.: Astrophys. J. **711**, 1029 (2010)
Saito, K., Poland, A.I.. Munro, R.H.: Sol. Phys. **55**, 121 (1977)
Sheeley, N.R. Jr., Hakala, W.N., Wang, Y.M.: J. Geophys. Res. **105**, 5081 (2000)
Smerd, S.F., Sheridan, K.V., Stewart, R.T.: In: Newkirk, G.A. (ed.) IAU Symp. 57, Coronal Disturbances, p. 389 Reidel, Dordrecht (1974)
Spangler, S.R.: Space Sci. Rev. **121**, 189 (2005)
Vasanth, V., Umapathy, S., Vrsnak, B., Zic, T., Prakash, O.:. (2013) (online)
Vourlidas, A., Wu, S.T., Wang, A.H., Subramanian, P., Howard, R.A.: Astrophys. J. **598**, 1392 (2003)
Vrsnak, B., Magdalenic, J., Aurass, H., Mann, G.: Astron. Astrophys. **396**, 673 (2002)
Vrsnak, B., Magdalenic, J., Zlobec, P.: Astron. Astrophys. **413**, 753 (2004)
Wiegelmann, T.: J. Geophys. Res. **113**, A03S02 (2008)